11th World Congress on Computational Mechanics (WCCM XI)
5th European Conference on Computational Mechanics (ECCM V)
6th European Conference on Computational Fluid Dynamics (ECFD VI)
E. Oñate, J. Oliver and A. Huerta (Eds)

XFEM-SIMULATION OF HYDRAULIC FRACTURING IN 3D WITH EMPHASIS ON STRESS INTENSITY FACTORS

Thomas-Peter Fries[1], Markus Schätzer[1], Nikolai Weber[2]

[1] Institute of Structural Analysis, Graz University of Technology,
Lessingstr. 25/II, 8010 Graz, Austria
e-mail: fries@tugraz.at, web page: http://www.ifb.tugraz.at

[2]Chair for Computational Analysis of Technical Systems, RWTH Aachen University,
Schinkelstr. 2, 52062 Aachen, Germany
e-mail: weber@cats.rwth-aachen.de, web page: http://www.cats.rwth-aachen.de

Key words: XFEM, 3D fracture, hydraulic fracturing

Abstract. The computation of stress intensity factors (SIFs) in the context of hybrid explicit-implicit crack descriptions is discussed. The *explicit* description is realized by surface meshes and is useful for the crack updates during propagation. The *implicit* description by level set functions is obtained from the surface meshes and is used for the XFEM approximation of displacements and stresses. SIFs are then computed by fitting the approximated fields. Different fitting approaches based on the hybrid crack description are investigated in 2D and 3D for applications in hydraulic fracture. An advantage of these approaches is that they work efficiently even for determining SIFs of curved cracks.

1 INTRODUCTION

Hydraulic fracturing (HF) is a process where a fracture initiates and propagates due to pressure exerted by the fluid inside the fracture. This process may take place naturally as e.g. in buoyant magma flows or for evolving cracks in dams. But the vast interest in engineering stems from the fact that artificially induced fracturing stimulates the flow in hydrocarbon (oil, gas) and geothermal reservoirs improving the production. Other applications include block-caving processes used in mining, waste disposal, carbon sequestration, and remediation of contaminated soils.

A number of physical processes are involved in a fluid driven fracture: The rock deformation due to the induced fluid pressure on the crack faces, the fluid flow within the fracture, and the fracture propagation [1]. Thermal and chemical effects are neglected here, since the focus of this work is fracture creation in 3D. These physical processes are modeled separately and solved within an iterative coupling. The strongly non-linear and non-local behavior makes hydraulic fracture modeling a challenging task. The extended

finite element method (XFEM) is used to deal with discontinuities and singularities which are present in this problem due to the existence of a (fluid-filled) crack. In XFEM, additional problem-specific functions (enrichments) are added to the approximation space to account for non-smooth solutions [3, 10, 8]. Furthermore, a hybrid explicit-implicit crack description is chosen which is beneficial in simulating hydraulic fracture propagation. An implicit description by means of level-sets is employed to determine the rock deformation. In contrast, a triangular surface mesh is used to describe the crack explicitly and to perform the crack update upon propagation. Another advantage of the explicit crack description in hydraulic fracture problems is that the fluid flow model is solved on the surface mesh which can be a potentially curved manifold within the three dimensional domain [7].

In this work, a particular focus is on the efficient and reliable extraction of stress intensity factors (SIFs). They define the stress and displacement fields in the neighborhood of a crack tip and are used as crack propagation criteria. There is a large number of literature on different approaches. We mention energy based methods such as those based on the J- or interaction integral, see e.g. [14, 13, 11]. Another class of methods studies the displacement or stress fields at the crack tip, among them the displacement extrapolation or fitting approaches, see e.g. [6, 9].

The paper is organized as follows: In Section 2, the governing equations for a hydraulic fracture problem in its basic form are presented. Models are discussed for the solid deformation, fluid flow, and fracture propagation. In Section 3, the XFEM formulation with an explicit-implicit crack description is described. Different approaches for the reliable evaluation of stress intensity factors are discussed in Section 4. Numerical results are presented in Section 5.

2 GOVERNING EQUATIONS

The equations governing hydraulic fracture must account for the three main physical phenomena of fluid flow, solid deformation, and fracture propagation. A strongly coupled partitioned approach is used for the solution of the coupled problem.

2.1 Rock deformation

The rock is modeled as a homogenous, isotropic, linear elastic solid. The material parameters quantifying the deformation process correspond to the Young's modulus E, Poisson's ratio ν, and rock toughness k_{IC}. The equations for the equilibrium of forces are given by:

$$\nabla \cdot \boldsymbol{\sigma} + \boldsymbol{f} = 0 \text{ in } \boldsymbol{\Omega},\ \boldsymbol{u} = \boldsymbol{u}_0 \text{ on } \boldsymbol{\Gamma}_d,\ \boldsymbol{\sigma} \cdot \boldsymbol{n} = \hat{\boldsymbol{t}}_n \text{ on } \boldsymbol{\Gamma}_n,\ \boldsymbol{p} \cdot \boldsymbol{n} = \hat{\boldsymbol{t}}_I \text{ on } \boldsymbol{\Gamma}_I \tag{1}$$

where $\boldsymbol{u}$ denotes the displacement defined on the domain Ω. Far field stresses and the fluid pressure p are imposed as Neumann boundary conditions at the outer boundary Γ_n and on the interface Γ_I, respectively, where $\hat{t}_n$ and $\hat{t}_I$ denote the traction. The fracture aperture w has to be interpolated from the displacement field.

2.2 Fluid flow

The model for the fracturing fluid is derived from Poiseuille equation as laminar flow between two parallel plates. It is valid for fractures with a crack length much larger than the width. With the assumption of an incompressible, Newtonian fluid, the Reynolds (lubrication) equation [2] is given by:

$$\frac{\partial w}{\partial t} - \boldsymbol{\nabla} \cdot \boldsymbol{q} + q_l = Q_0 \delta(\boldsymbol{x}) \quad \text{with} \quad \boldsymbol{q} = -\frac{w^3}{12\mu} \boldsymbol{\nabla} p \tag{2}$$

and describes the conservation of the fluid mass with the dynamic viscosity μ. The fluid is injected into the fracture at a constant rate Q_0 and is incorporated as a point source into the model since the borehole is not considered in this study. Furthermore, the fracture is propagating in an impermeable solid, and thus, the leak-off term q_l is negligible. Finally, the fracture volume V is equated to the volume of injected fluid $V_f = Q_0 t$ and the amount lost to the surrounding rock-mass by the global volume balance condition:

$$V = \int_\Omega w \, \mathrm{d}\Omega = V_f - \int_0^t \int_\Omega q_l \, \mathrm{d}\Omega \, \mathrm{d}\tau. \tag{3}$$

2.3 Fracture propagation

In this work, a quasi-static crack growth is assumed and the crack propagates continuously under mobile equilibrium. In general, a number of various propagation criteria could be applied to this problem. These include local conditions based on stress intensity factors or the stress state in the vicinity of the crack front as well as conditions derived from global energy considerations. In this study, the focus is on extracting stress intensity factors by fitting displacements or stresses in the near-tip region. In terms of numerical implementation, only one node at the crack front has to fulfill the critical condition $k_I = k_{IC}$, which states that the stress intensity factor k_I has to be equal to the fracture toughness k_{IC} of the material [12]. The direction of crack propagation is then calculated from the maximum circumferential stress criterion.

3 XFEM WITH HYBRID EXPLICIT-IMPLICIT CRACK DESCRIPTION

The extended finite element method (XFEM) is a local partition of unity (PU) based method, which accounts for a priori knowledge about the solution characteristics by locally incorporating enrichment functions into the finite element approximation space. Thereby, fields that involve jumps, kinks, singularities, and other non-smooth features within elements can be approximated accurately [3, 10, 8]. In linear elastic fracture mechanics, the standard XFEM formulation for the displacement approximation is:

$$\boldsymbol{u}^h(\boldsymbol{x}) = \underbrace{\sum_{i \in I} \boldsymbol{N}_i \, \boldsymbol{u}_i}_{\text{continuous}} + \underbrace{\sum_{j \in I^{step}} \boldsymbol{N}_j^\star \cdot \Psi_{step} \, \boldsymbol{a}_j + \sum_{k \in I^{tip}} \boldsymbol{N}_k^\star \cdot \left(\sum_{m=1}^{4} \Psi_{tip}^m(r,\theta) \, \boldsymbol{b}_k^m \right)}_{\text{discontinuous}} \tag{4}$$

The classical FEM-approximation is described by the continuous part of the equation with continuous shape functions $\boldsymbol{N}_i(\boldsymbol{x})$ and nodal unknowns $\boldsymbol{u}_i$. Discontinuous characteristics across the crack path in the displacement field are accounted for by incorporating locally step or Heaviside functions Ψ_{step} and additional nodal unknowns $\boldsymbol{a}_j$ at nodes within the set I^{step}. Nodes within I^{tip} are enriched with a set of four enrichment functions $\Psi^m_{tip}(r,\theta)$ which capture the square-root singularity according to the linear elastic fracture mechanics (LEFM) theory. Additional degrees of freedom $\boldsymbol{b}^m_k$ are introduced into the approximation locally within the enriched region.

The strong fluid-solid coupling in hydraulic fracture problems that is mainly confined to a small region near the crack tip [5] influences the choice of the tip enrichment functions. For a fluid-filled crack propagating in an impermeable rock, two limiting energy dissipation processes can by identified: the work done by the viscous fluid in extending a fracture and the energy required to create new crack surfaces. In the toughness dominated propagation regime, the dissipation energy for fracture creation is dominant and the effect of the crack tip process on the total fracture is described by the inverse square root singularity of LEFM [4].

3.1 Explicit-implicit interface description

An explicit crack description simplifies the crack update during the propagation. On the other hand, an implicit crack description by the level-set method complements the XFEM extremely well and is a standard in XFEM ever since. The aim is to combine the advantages of each description, see [7] for further details. Three level-set functions are defined which allow not only for determining the crack location but enable the definition of a local coordinate system at the crack front, see Figure 1.

- $\Phi_1(\boldsymbol{x})$ is the (un-signed) distance function to the crack path/surface. That is, the level-set value at position $\boldsymbol{x}$ is the shortest distance to the crack path/surface.
- $\Phi_2(\boldsymbol{x})$ is the (un-signed) distance function to the crack tip(s)/front. That is, the level-set value at position $\boldsymbol{x}$ is the shortest distance to the crack tip(s)/front.
- $\Phi_3(\boldsymbol{x})$ is a signed distance function to crack path/surface that is extended over the whole domain. The sign is based on the direction of the normal vector of the segment that contains the nearest point.

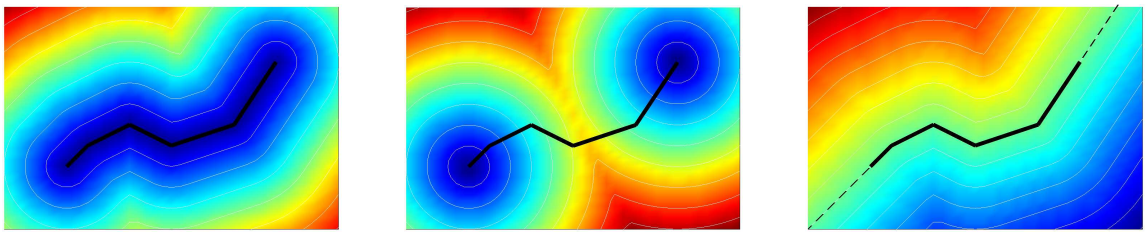

(a) $\Phi_1(\boldsymbol{x})$ (b) $\Phi_2(\boldsymbol{x})$ (c) $\Phi_3(\boldsymbol{x})$

Figure 1: The level-set functions are illustrated for a 2D case [7].

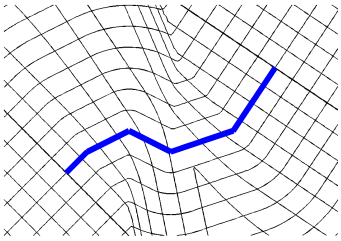

(a) The coordinate system (a, b)

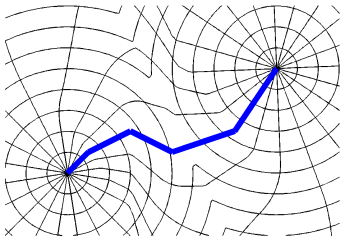

(b) The coordinate system (r, θ)

Figure 2: Coordinate systems implied by the three level-set functions [7].

These level-set functions imply coordinate systems, which are used to define the regions to be enriched and to evaluate the enrichment functions. See Figure 2 for two different particularly useful coordinate systems. It is a major advantage of the described explicit-implicit crack description that the extension to 3D is truely straightforward as shown in [7]. In the next section, it is discussed how to extract stress intensity factors based on the coordinate system (a, b).

4 COMPUTING STRESS INTENSITY FACTORS

The state at the crack tip is completely described by a linear combination of the crack modes plus a rigid body motion. The factors of this linear combination are called SIFs. As mentioned before, there are local and global approaches for determing SIFs. Here, the focus is on fitting SIFs based on displacements or stresses.

4.1 The approximated state

The approximated state in terms of displacements, stresses, and strains is given as a result of an XFEM simulation (or by a classical FEM simulation on a suitable mesh). The crack is closed in the undeformed configuration and given by an explicit line or surface mesh in 2D or 3D, respectively. Based on this explicit description, we compute two scalar functions $a(\boldsymbol{x})$ and $b(\boldsymbol{x})$ from the three level set functions as mentioned above.

In 2D, the two functions a and b define a coordinate system with base vectors $\boldsymbol{e}_a$ and $\boldsymbol{e}_b$ defined as

$$\boldsymbol{e}_a = \mathbf{J}^{-1} \begin{bmatrix} 0 \\ 1 \end{bmatrix}, \; \boldsymbol{e}_b = \mathbf{J}^{-1} \begin{bmatrix} 1 \\ 0 \end{bmatrix}, \text{ with } \mathbf{J} = \begin{bmatrix} a_{,x} & a_{,y} \\ b_{,x} & b_{,y} \end{bmatrix}. \tag{5}$$

These base vectors are shown in Figure 3(a). Only for planar cracks, they have unit-length (measured in the $\boldsymbol{x}$-coordinate system) and are orthogonal.

After the deformation of the body (with a potential opening of the crack) the base

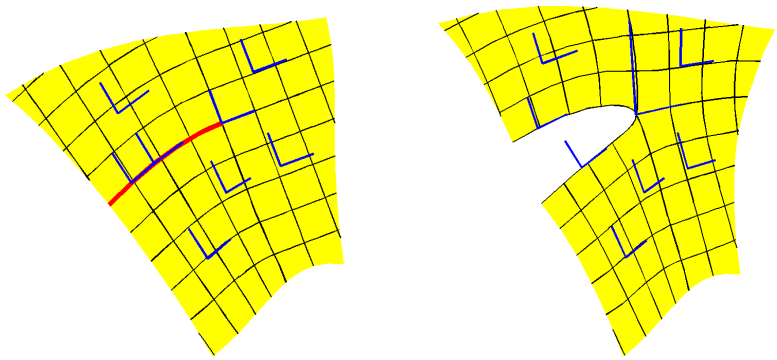

(a) Undeformed configuration. (b) Deformed configuration.

Figure 3: The coordinate systems defined by the two scalar functions $\boldsymbol{a}$ and $\boldsymbol{b}$ in the (a) undeformed and (b) deformed configuration. The vectors $\boldsymbol{e}_a$ and $\boldsymbol{e}_b$ are shown examplarily at some points.

vectors are transformed by means of the deformation gradient $\mathbf{F}$ as

$$\boldsymbol{e}_a^\star = \mathbf{F} \cdot \boldsymbol{e}_a, \; \boldsymbol{e}_b^\star = \mathbf{F} \cdot \boldsymbol{e}_b, \text{ with } \mathbf{F} = \begin{bmatrix} 1+u_{,x} & u_{,y} \\ v_{,x} & 1+v_{,y} \end{bmatrix}. \tag{6}$$

These mapped base vectors are shown in Figure 3(b).

In 3D, the *two* functions a and b define the *three* base vectors $\boldsymbol{e}_a$, $\boldsymbol{e}_b$, and $\boldsymbol{e}_c$. Therefore, we first compute $\nabla c = \nabla a \times \nabla b$, so there is no need to explicitly define a third function $c(\boldsymbol{x})$. Then,

$$\boldsymbol{e}_a = \mathbf{J}^{-1} \begin{bmatrix} 1 \\ 0 \\ 0 \end{bmatrix}, \; \boldsymbol{e}_b = \mathbf{J}^{-1} \begin{bmatrix} 0 \\ 1 \\ 0 \end{bmatrix}, \; \boldsymbol{e}_c = \mathbf{J}^{-1} \begin{bmatrix} 0 \\ 0 \\ 1 \end{bmatrix}, \text{ with } \mathbf{J} = \begin{bmatrix} a_{,x} & a_{,y} & a_{,z} \\ b_{,x} & b_{,y} & b_{,z} \\ c_{,x} & c_{,y} & c_{,z} \end{bmatrix}.$$

The mapping of the base vectors to the deformed configuration is achieved by means of the 3D deformation gradient following Eq. (6). See Figure 4 for a visualization.

It is noted that the mapped base vectors will later only be needed at the crack tip and along the crack path but not in the bulk.

4.2 Reference states

In order to fit the SIFs, reference states for the individual crack modes are needed. Apparently, the undeformed configuration does not involve the displacements that may occur even in the absence of a crack opening (composed by the crack modes). The crack tip typically experiences a translation and rotation in addition to the opening of the crack modes. If we wish to express the displacement field at the crack tip solely in terms of the crack modes, i.e.

$$\boldsymbol{u}(\boldsymbol{x}) = \boldsymbol{u}_I(\boldsymbol{x}) \cdot k_I + \boldsymbol{u}_{II}(\boldsymbol{x}) \cdot k_{II} + \boldsymbol{u}_{III}(\boldsymbol{x}) \cdot k_{III}, \tag{7}$$

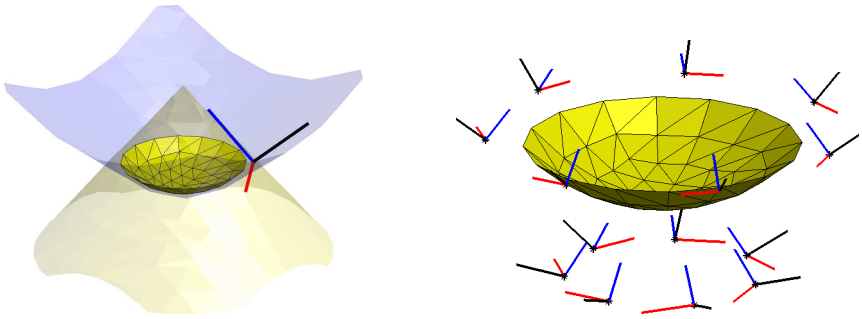

(a) (b)

Figure 4: (a) For a selected point $\boldsymbol{x}^\star$, the corresponding isosurfaces where $\boldsymbol{a} = \boldsymbol{a}(\boldsymbol{x}^\star)$ and $\boldsymbol{b} = \boldsymbol{b}(\boldsymbol{x}^\star)$ are shown. Furthermore, the resulting base vectors are depicted at that point. (b) Other base vectors for selected points.

we have to make sure that the movement of the crack tip that is not related to the crack opening is filtered out properly. Therefore, the reference state is composed by a *virtual*, deformed configuration without any crack opening. The reference state is associated with a coordinate system (a', b') in which the crack modes (with $k_I = k_{II} = k_{III} = 1$, respectively) are evaluated and then used in the fitting procedure described below.

Three different virtual configurations are considered here:

- Reference state 1 refers to a coordinate system (a', b') at the crack tip which is defined through the crack center line of the open crack. The position of this line is composed by the midpoints between any two points on the crack surface that have been adjacent in the undeformed configuration. Then, three level set functions are computed with respect to this deformed (yet closed) crack surface and the scalar functions a' and b' are computed accordingly.

- Reference state 2 is a rigid body motion of the coordinate system (a, b) (and hence, the original closed crack) solely defined by the crack tip movement. The coordinate system is curved when the crack is already curved in the undeformed configuration.

- Reference state 3 refers to an orthonormal coordinate system (a', b') based on the tangential deformed crack tip direction $\boldsymbol{e}_a^\star$. The associated virtual crack path would be a straight line where the angle is solely determined by the crack tip rotation.

These reference states, i.e., the related coordinate systems are shown in Figure 5(a) to (c). The black lines are the isolines of the scalar functions a and b and indicate the coordinate system. The red line is the associated virtual crack path where $b = 0$ and $a < 0$. The dashed black line is the approximated crack opening in the deformed configuration.

Figure 6 shows a pure mode I and II opening with $k_I = k_{II} = 1$, evaluated in the coordinate system (a', b'). The displacements u' and v' are obtained in the directions of $\boldsymbol{e}_a'$ and $\boldsymbol{e}_b'$ (the latter are defined as in Eq. (5) but with the scalar functions a' and b').

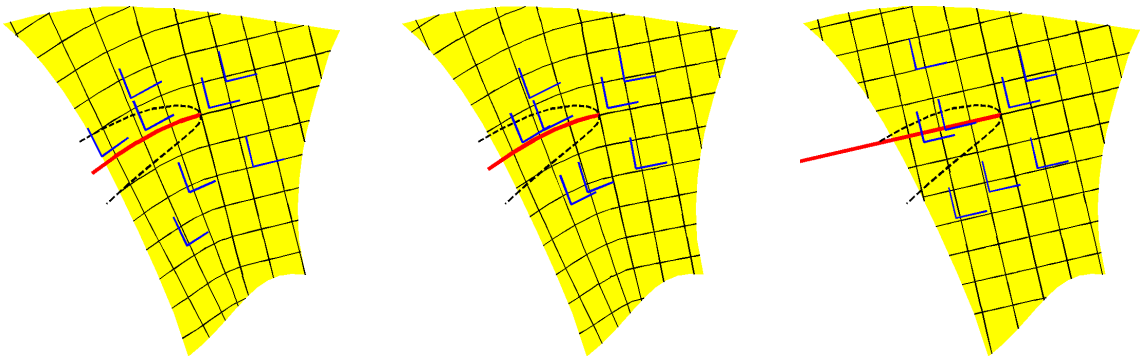

(a) Reference state 1. (b) Reference state 2. (c) Reference state 3.

Figure 5: The coordinate systems of different reference states. The dashed black line is the open crack path. The red line is the crack path according to the reference state.

For the relation between displacements in the (x, y)- and (a', b')-coordinate system holds

$$\begin{bmatrix} u \\ v \end{bmatrix} = u' \cdot \boldsymbol{e}'_a + v' \cdot \boldsymbol{e}'_b. \tag{8}$$

For any evaluation point $\boldsymbol{x}$ in the fitting procedures described below, the following steps are performed: (1) The scalar functions $a(\boldsymbol{x})$ and $b(\boldsymbol{x})$ are evaluated. (2) The point $\boldsymbol{x}^\star = \boldsymbol{x} + \boldsymbol{u}^h(\boldsymbol{x})$ is computed. (3) The point $\boldsymbol{x}'$ where $a'(\boldsymbol{x}') = a(\boldsymbol{x})$ and $b'(\boldsymbol{x}') = b(\boldsymbol{x})$ is determined. This is simple for reference states 2 and 3, but rather cumbersome for state 1. The basis vectors $\boldsymbol{e}'_a$ and $\boldsymbol{e}'_b$ at that point are computed. (4) The displacements $\boldsymbol{u}'_I$ and $\boldsymbol{u}'_{II}$ according to a pure mode I and II crack (with $k_I = k_{II} = 1$) are evaluated. (5) The displacement $\left(\boldsymbol{u}^h\right)'$ between $\boldsymbol{x}'$ and $\boldsymbol{x}^\star$ is computed in the direction of $\boldsymbol{e}'_a$ and $\boldsymbol{e}'_b$. For brevity, the prodecure is described for displacements, but works analogously for stress components. The extension to 3D is straightforward.

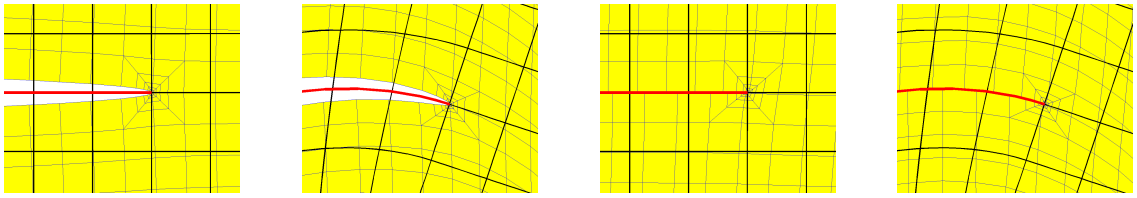

(a) $k_I = 1$, planar (b) $k_I = 1$, curved (c) $k_{II} = 1$, planar (d) $k_{II} = 1$, curved

Figure 6: Crack modes in the reference states, (a) and (c) for a planar crack path, (b) and (d) for a curved crack path. The black lines indicate the reference coordinate system (a', b').

4.3 The fitting procedure

The aim is to determine the unknown SIFs which are two unknowns in 2D and three in 3D. The answer could be provided by only one evaluation point and comparing the

reference and approximated states. However, it is benefitial to consider a larger number of points in the vicinity of the crack tip. Then, the SIFs are determined through fitting. We distinguish between fitting displacements and stresses.

4.3.1 Fitting quantities

The fitting may be realized in a weak sense or through an overdetermined system. This is exemplarily shown for the fit of the displacement component u' in $\boldsymbol{e}'_a$-direction:

Alternative 1: The following weak form is evaluated in the crack tip zone

$$\int \begin{bmatrix} u'_I \cdot u'_I & u'_I \cdot u'_{II} \\ u'_{II} \cdot u'_I & u'_{II} \cdot u'_{II} \end{bmatrix} \mathrm{d}\Omega \cdot \begin{bmatrix} k_I \\ k_{II} \end{bmatrix} = \int \begin{bmatrix} u'_I \cdot \left(u^h\right)' \\ u'_{II} \cdot \left(u^h\right)' \end{bmatrix} \mathrm{d}\Omega \tag{9}$$

Alternative 2: The equation $u'_I \cdot k_I + u'_{II} \cdot k_{II} = \left(u^h\right)'$ is evaluated at $n > 2$ points yielding an overdetermined system of equations $\mathbf{A} \cdot [k_I,\ k_{II}]^{\mathrm{T}} = \boldsymbol{b}$, where $\mathbf{A}$ is an $(n \times 2)$-matrix. Then, the system is solved in a least squares sense, i.e.

$$\mathbf{A}^{\mathrm{T}}\mathbf{A} \cdot \begin{bmatrix} k_I \\ k_{II} \end{bmatrix} = \mathbf{A}^{\mathrm{T}}\boldsymbol{b} \tag{10}$$

It appears more natural to determine k_I by fitting the displacement component in $\boldsymbol{e}'_b$-direction, i.e. through v'_I, v'_{II}, and $\left(v^h\right)'$ because this is the more pronounced component for the *opening* mode. Accordingly, k_{II} (shearing mode) should be fitted from u'_I, u'_{II}, and $\left(u^h\right)'$ and k_{III} (tearing mode) from w'_I, w'_{II}, and $\left(w^h\right)'$.

Finally, it is noted that instead of fitting displacements one may also use stresses. Then, k_I is determined through σ'_{bb}, k_{II} through σ'_{aa}, and k_{III} through σ'_{cc}.

4.3.2 Fitting locations

For the two fitting alternatives discussed above, it remains to specify *where* evaluation points are considered. Different approaches are investigated:

Fitting the crack opening displacements Evaluation points are put on the crack surface, i.e. on the two sides of the zero-iso-level. For each pair of adjacent points, the displacement components with respect to the averaged crack center line are determined. This gives the components for opening, shearing and tearing. Together with the distance to the crack front, the SIFs can be determined pointwise and averaged if desired.

Fitting the displacements near the crack tip zone A radius around the crack tip defines the domain Ω where all integration points contribute to the weak form (9).

Fitting the stresses near the crack tip zone When fitting stresses, an inner and outer radius are specified and the integral (9) is evaluated on a torus around the crack tip. This avoids the consideration of the nearly singular stresses near the crack tip.

Fitting the displacements on circles Instead of evaluating an integral in the bulk, one may also define a circle around the crack tip and place evaluation points on the circle. Then, we solve (10) in order to fit displacements.

Fitting the stresses on circles Again, evaluation points on a circle with a prescribed radius are placed around the crack tip. Then, the SIFs are obtained by fitting the stress compenent $\sigma'_{r\theta}$ in a polar coordinate system. The polar coordinates are easily obtained from the (a', b')-coordinate system. The advantage of this approach is that only an arc of the circle in front of the crack tip can be considered. In that region, the three reference states coincide.

5 NUMERICAL RESULTS

For the comparison of the different alternatives for fitting the SIFs, a well-known test case in hydraulic fracturing is chosen where the exact solution is known. In 2D, a planar crack is considered in an infinite domain. For the discrete setup, the ratio of the crack and the boundary of the domain is 1:40. For symmetry reasons, only half of the domain is considered. A sketch of the discretized domain and a detailed region along the crack path are shown in Figure 7. Results are obtained with both classical FEM simulations on conforming meshes and XFEM simulations with the described hybrid explicit-implicit crack description.

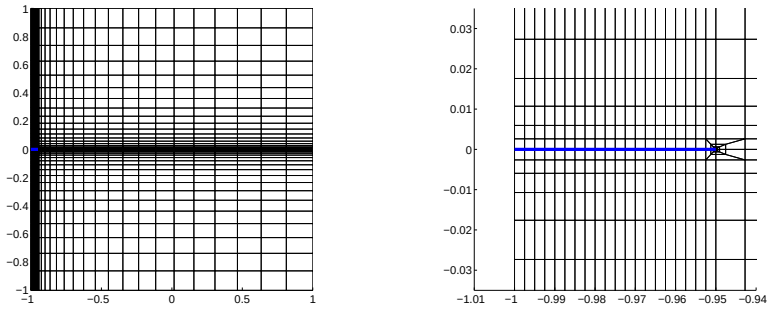

(a) domain (b) detail

Figure 7: The test case is 2D.

The crack opening and the resulting SIFs are known analytically for arbitrary pressure profiles along the straight crack. Here, we choose a constant, linear and quadratic pressure profile. The resulting crack opening profiles and SIFs are given in Figure 8.

Convergence results for different fitting approaches are seen in Figure 9. Method 1 is the fitting of displacements is the bulk region at the crack tip for different radii, see Figure 9(a) to (c). The stress fit in the near-tip region is called method 2, see Figure 9(d) to (f). Finally, results are shown for method 3, where stresses on an arc near the crack tip are shown for different radii, see Figure 9(g) to (i).

In 3D, the fluid filled penny shape crack is considered in an infinite domain. Again, different pressure profiles and fitting approaches are investigated. The results are discussed

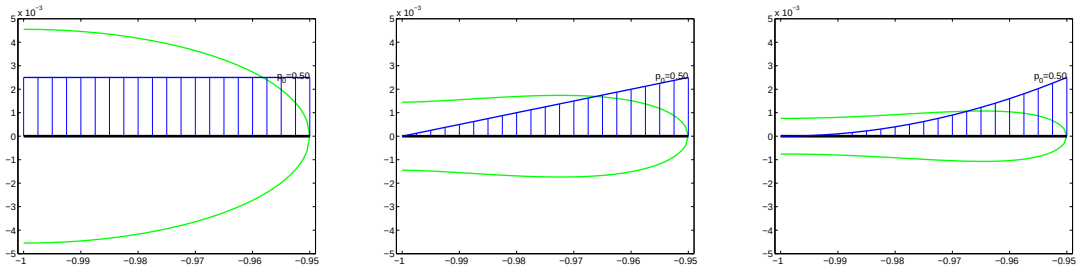

(a) constant pressure, $k_I = 0.1982$ (b) linear pressure, $k_{II} = 0.1262$ (c) quadratic pressure, $k_{III} = 0.0991$

Figure 8: Crack opening profiles and SIFs for different pressures.

in the presentation and are to be published in a forth-coming journal publication.

REFERENCES

[1] J. Adachi, E. Siebrits, A. Peirce, and J. Desroches. Computer simulation of hydraulic fractures. *Int. J. Rock Mech. Min. Sci.*, 44(5):739 – 757, 2007.

[2] G. Batchelor. *An Introduction to Fluid Dynamics*. Cambridge University Press, 1967.

[3] T. Belytschko and T. Black. Elastic crack growth in finite elements with minimal remeshing. *IJNME*, 45:601 – 620, 1999.

[4] A. Bunger, E. Detournay, D. Garagash, and A. Peirce. Numerical simulation of hydraulic fracturing in the viscosity dominated regime. In *SPE Hydraulic Fracturing Technology Conference*, 2007.

[5] E. Detournay. Fluid and solid singularities at the tip of a fluid-driven fracture. In D. Durban and J. Pearson, editors, *IUTAM Symposium on non-linear singularities in deformation and flow, Proceedings*, pages 27–42, 1999.

[6] C. Duarte, O. Hamzeh, T. Liszka, and W. Tworzydlo. A generalized finite element method for the simulation of three-dimensional dynamic crack propagation. *Engineering Fracture Mechanics*, 72:1635 – 1663, 2005.

[7] T.-P. Fries and M. Baydoun. Crack propagation with the extended finite element method and a hybrid explicit–implicit crack description. *Int. J. Num. Meth. Engng.*, 89(12):1527–1558, 2012.

[8] T.-P. Fries and T. Belytschko. The extended/generalized finite element method: An overview of the method and its applications. *Int. J. Num. Meth. Engng.*, 84(3):253–304, 2010.

[9] A. Ingraffea and C. Manu. Stress-intensity factor computation in three dimensions with quarter-point elements. *Numerical Methods in Engineering*, 15:1427 – 1445, 1980.

[10] N. Moës, J. Dolbow, and T. Belytschko. A finite element method for crack growth without remeshing. *IJNME*, 46:131 – 150, 1999.

[11] J. Pereira and C. Duarte. The contour integral method for loaded cracks. *Numerical Methods in Biomedical Engineering*, 22:421 – 432, 2006.

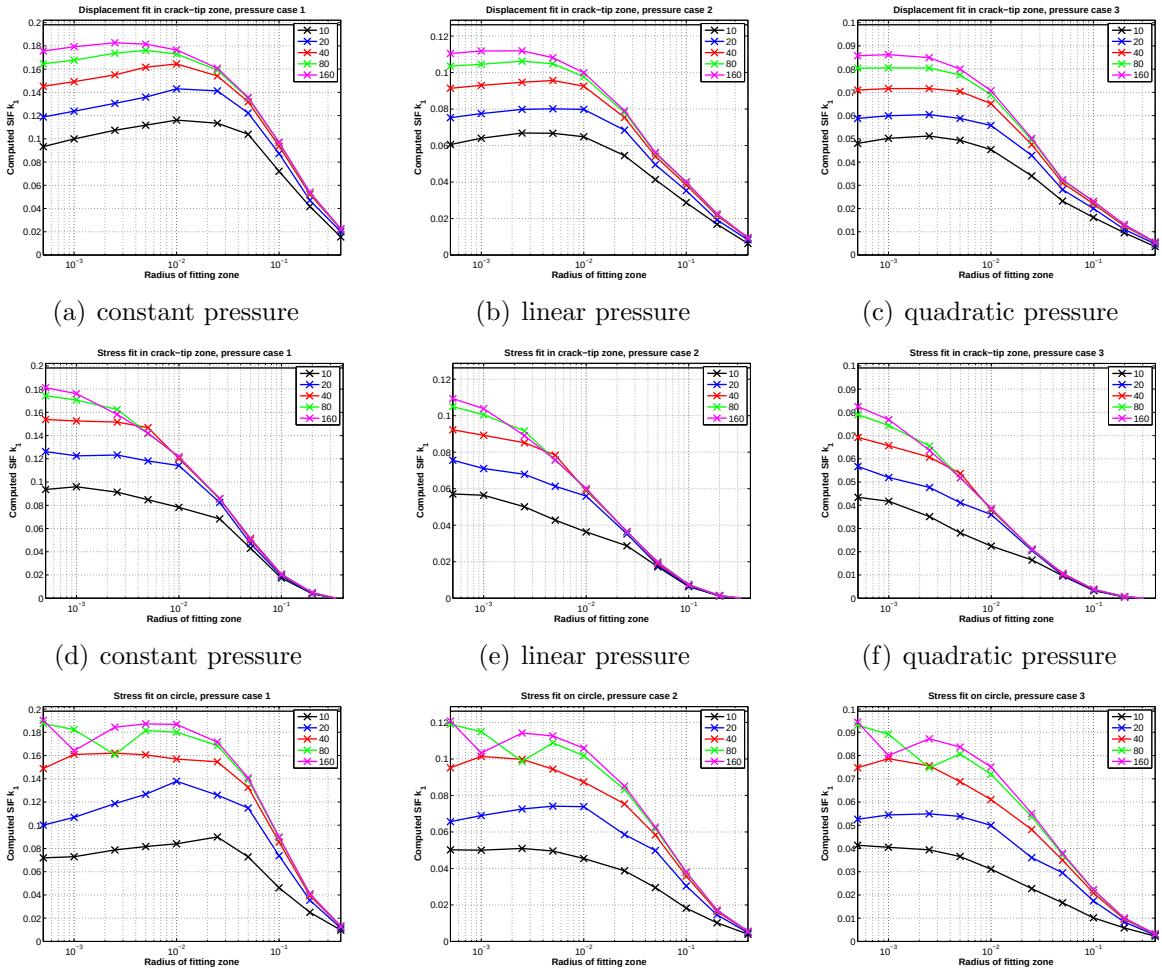

(a) constant pressure (b) linear pressure (c) quadratic pressure

(d) constant pressure (e) linear pressure (f) quadratic pressure

(g) constant pressure (h) linear pressure (i) quadratic pressure

Figure 9: Convergence of the fitting approaches in the near-tip region with different radii.

[12] J. Rice. Mathematical analysis in the mechanics of fracture. In H. Liebowitz, editor, *Fracture: An Advanced Treatise*, volume 2 of *Mathematical Fundamentals*, chapter 3, pages 191–311. Academic Press, New York, 1968.

[13] M. Walters, G. Paulino, and R. Doods. Interaction integral procedures for 3-d curved cracks including surface tractions. *Engineering Fracture Mechanics*, 72:1635 – 1663, 2005.

[14] L. Wu, L. Zhang, and Y. Guo. Extended finite element method for computation of mixed-mode stress intensity factors in three dimensions. *Procedia Engineering*, 31:373 – 380, 2012.